Civil Engineering and Smart Structure Technology
W. Yao et al. (Eds.)

doi:10.3233/ATDE250195

Analysis on Stress State of Arch Complex Joints of Long-Span Underpass Composite Bridge

Ziyi HUANG[a], Hao HUANG[a], Huajun LIAO[b], Diandong SUN[c] and Wei WANG[c,1]
[a]*Jiangxi Province Yingtan City Housing and Urban-Rural Development Bureau, Yingtan 335000, Jiangxi, China*
[b]*Jiangxi Yingtan City Highway Development Center, Yingtan 335000, Jiangxi, China*
[c]*Changchun Institute of Technology, Changchun 130012, Jilin, China*

Abstract. In order to analyze the stress and strain state of the arch consolidated complex joint of the long-span beam arch combined bridge, the spatial stress distribution of the arch beam joint of Yuehu super Bridge is studied. Through the three-dimensional finite element model and the scaled solid model, the stress behavior of the joint part of the arch foot is analyzed. The results show that the maximum edge stress of the main beam is 249.5MPa, and the stress at the root of the arch rib is diffused. The overall deformation gradually increases towards the root of the arch rib. The maximum deformation is 3.6cm at the root of the arch rib, and the overall deformation gradually increases from the junction to the root of the arch rib. The load test is in good agreement with the finite element results. The cast-in bridge panel has no obvious buckling and cracks, and the structural force is reasonable, meeting the requirements of the code. It has important theoretical and practical significance to provide reference for similar projects.

Keywords. Bridge, beam and arch combination, complex node, simulation, experiment

1. Introduction

China's arch bridge has a long history, carries a rich cultural tradition, and is also a world record holder, and its design and construction technology has become more and more mature [1]. In modern bridge design, arch bridge is favored by designers because of its beautiful curves, but its design difficulty and construction technology requirements are also significant, especially the key part of the arch foot. The arch foot not only needs to bear the full load of the bridge, but also needs to transfer the load to the support, and its importance is self-evident.

In order to better understand and solve the problems of arch bridge design and construction, scholars at home and abroad have carried out a lot of research work. They used a variety of research methods, including theoretical analysis [2-4], finite element simulation [5-7], and large-scale construction scale experiments [8]. For example, Sun and Miao [9] used finite element analysis software to simulate the continuous beam-arch combined bridge in actual engineering, analyzed the change trend of the

[1] Corresponding Author: Wei Wang, 16695496@qq.com

cable force value of the derrick in each construction stage, and summarized the basic consistency of the internal force of the main beam and arch rib under different load conditions. Zheng [10] calculated and analyzed the static and dynamic effects of a continuous beam-arch combined bridge, and put forward suggestions for stress optimization of the arch girder combined section.

Dai [11] took a continuous beam arch composite bridge along the Lan-yu line as an example, studied the seismic response rule of the bridge, and analyzed the damping performance of the bridge after setting the speed locking device, considering the pile-soil interaction [12]. Zhang [13] proposed a number of optimization measures for Xuhonghe Bridge to solve the structural problems [14]. Gong [15] and Zhang [16] found that stress concentration exists in continuous rigid frame Bridges, while Yu et al. [17] discussed the complex stress state in the consolidation area of tower pier beams of cable-stayed Bridges. However, the arch foot of a beam-arch composite system bridge is subject to more complex stress, which requires further research and discussion. There is an obvious stress concentration in the local arch foot, which may lead to the cracking of concrete [18]. As the key stress position of the tied arch bridge, the arch foot is very complex in structure, and special attention should be paid to it in the design process [19-20]. Therefore, it is very important to establish the local finite element solid calculation model of arch foot and carry out scaled model test for understanding its stress characteristics, analyzing stress law and guiding design and construction, which will help to improve the safety and reliability of arch foot of arch bridge.

To sum up, the stress on the complex joint of the beam arch consolidation is concentrated, and the cracking phenomenon is common in the construction and operation process. At present, there is no clear standard calculation formula to accurately calculate the mechanical performance of the beam arch joint structure. It is necessary to verify the safety and redundancy of the beam arch consolidated joint in the design scheme.

This paper is based on the Moon Lake Special Bridge with a downward-bearing beam-arch combination. By establishing a three-dimensional finite element model and a corresponding scaled physical model, it explores the spatial stress distribution law of the arch-foot joint part of the Moon Lake Special Bridge. The aim is to provide a reference for the design and construction of the bridge, ensure that the mechanical performance of the beam-arch consolidation joint meets the requirements, and this is of great significance for guaranteeing the operational safety of the overall bridge.

2. Project Overview

Yuehu Bridge is a downward arch bridge, and the joint of beam and arch is an important force transfer node of the structure, and the center line of the node is set with supports, which is the most prone to stress concentration of the whole bridge, and the safety of the node affects the safety of the whole bridge structure. In addition to the overall analysis of the bridge structure, it is also necessary to conduct local analysis of the beam arch joint to ensure the safety of the joint. Because of the symmetry of the bridge structure, only one of the beam arch nodes is selected for fine analysis. The GJa segment is selected for local fine force analysis. This node is the joint of the steel box arch and the main beam, and its position in the whole bridge structure is shown in Figure 1. The length of the main beam is 17.5m and the length of the arch rib is 11.6m. The main beam is provided with 9 transverse partitions, and the arch rib is provided with 4 transverse partitions. The web connecting position between the arch rib and the main beam is provided with a fly plate, and the web plate is provided above the support for strengthening. The joint consists of the intersection of arch rib and main beam, and adopts the construction mode of box section. The width of arch rib and tie beam is the same, both are 6.0m. A fly plate is arranged between the arch rib and the main beam, a steel backing plate is arranged above the support, and a web plate is specially arranged for local strengthening. The structure and main section design of nodes are shown in Figure 2. All steel plates are made of bridge structural steel Q345qD. According to the provisions of the Code for Design of Steel Structures (GB50017-2017), the mechanical properties of steel joints are shown in Table 1.

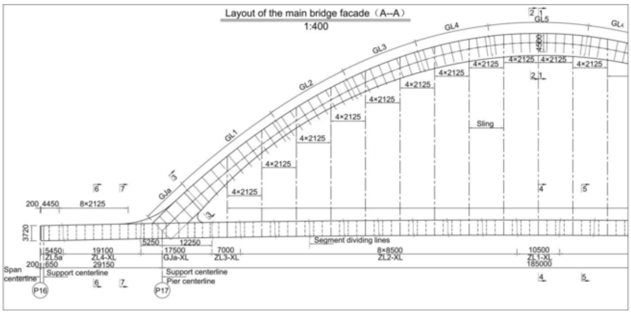

Figure 1. Location of nodes in the full bridge structure.

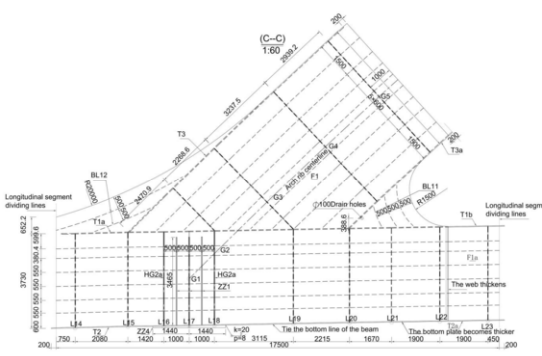

Figure 2. Front elevation of node structure.

Table 1. Design strength index of steel joints

Strength class	Modulus of elasticity	Tensile/compressive/bending resistance	shear
	E_s	f_s	f_v
Q345qD	2.06x105MPa	270MPa	155MPa

3. Calculation Model and Load Condition

3.1. Model Overview

The general finite element software ABAQUS was used to conduct detailed force analysis on the overall structure of Yuehu Bridge nodes. The models included main beams, bridge panels and arch rib segments. The finite element model of the nodes was shown in Figure 3. As a whole structure, the internal force derived by Midas software is used as the load input of the boundary section. Three-node and four-node shell elements were used to simulate the structure, and the nodes were divided into 170,000 units. The international system of Units is used in the calculation of the model. The unit of length is m and the unit of stress is Pa.

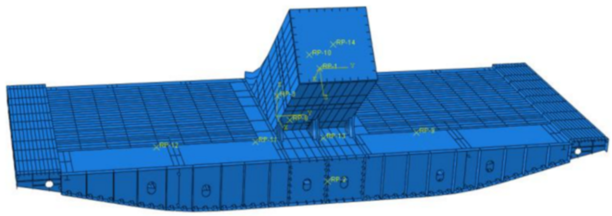

(a) Geometric model

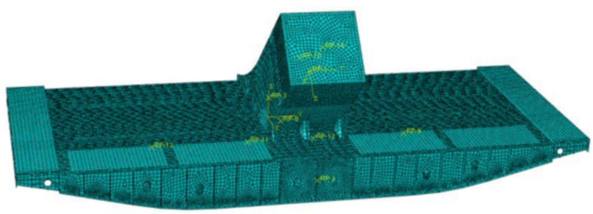

(b) Unit partition

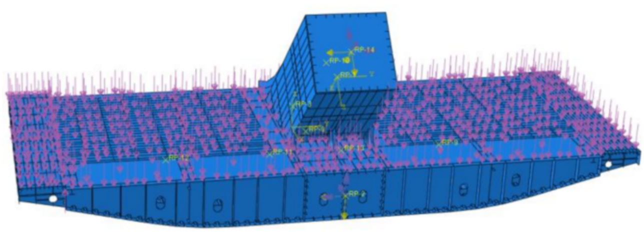

(c) Boundary load input

Figure 3. Finite element model of nodes

The boundary section is connected to the reference point through the reference point, and then the load is input to the reference point. When the arch rib section load is input, the local coordinate system should be established according to the direction of arch rib section, and the boundary section load should be input to the structure through the local coordinate system to ensure the correct direction of load. In order to be as close to the actual situation as possible, according to the design description of the construction drawing of Yuehu Bridge, the top surface of the fixed pier is equipped with a fixed spherical steel support, a transverse movable spherical steel support, and the top surface of the movable pier is equipped with a longitudinal movable spherical steel support and a two-way movable spherical steel support. The top of the transition pier is provided with longitudinal moving ball bearings and bidirectional moving ball bearings, and corresponding boundary conditions are set.

3.2. Load Condition

According to the provisions of the "General Code for the Design of highway Bridges and culverts" (JTGD60-2015) and the "Code for the design of steel-concrete composite Bridges" (GB50917-2013): "The function of stress checking calculation (or load) should be a standard combination. Among them, the vehicle load should be included in the impact factor." The local stress check calculation under the persistent condition adopts the following load combination: 1.1× [(dead weight + second stage) ×1.2+ shrinkage and creep ×1.2+ foundation displacement ×1.0+ vehicle load (including impact force) ×1.4+ (braking force + crowd load + overall rising and cooling + gradient temperature) ×1.4+ wind load ×1.1) ×0.5]. The distribution mode of arch foot bending moment as live load is used for analysis and calculation. To facilitate the input of external forces on nodes, the positions of contact points are numbered as shown in Figure 4. E and B represent the full section of the steel box girder, A represents the arch rib section, and D1-D4 represents the four supports.

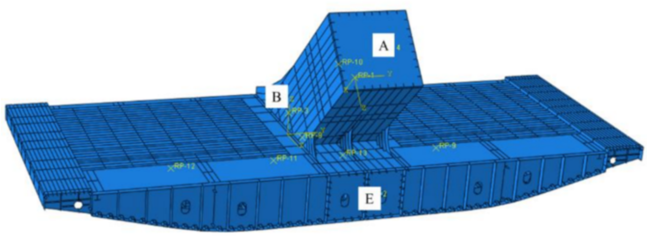

Figure 4. Model boundary section

The external force of the boundary section of the whole model of the beam arch joint when the arch foot has the most unfavorable bending moment. The axial force is positive for tension and negative for compression. The shearing force is positive along the local coordinate direction, and the direction of bending moment and torque is determined according to the right-hand spiral rule of the local coordinate direction. The external force input values of the section of the beam arch node are shown in Table 2

Table 2. External force input values of beam arch joint section

Internal force	Node B	Node E	Node A
Axial force Fx/kN	-37934	10226.89	-105219
Shearing force Fy/kN	-554.22	-4646.47	-578.11
Shearing force Fz/kN	10136.08	-3216.35	1929.69
Torque Mx (kN·m)	2582.79	-22403.1	-5895.48
Torque Mx(kN·m)	-47888.9	26759.92	12629.34
Torque Mx(kN·m)	418.91	4459.67	-20265.2

4. Analysis of Stress Behavior Combined with Parts

4.1. Joint Stress Analysis

The tensile and compressive stress distribution of the beam arch joint was shown in Figure 4, in which the steel plate was analyzed according to Von-mises stress cloud diagram. The results show that the maximum stress occurs on the web of the main beam and the transverse diaphragm above the support. Among them, due to the connection of reference points (couple), the boundary cross section may cause a large stress concentration phenomenon, and the stress results at this part can be ignored. The stress of the web of the main beam above the support and the bottom plate connected to it are not exceeded (more than 270MPa), and meet the requirements.

According to the finite element analysis results. In Figure 5. The beam arch joint will undergo certain stress changes under the action of load, and with the increase of load, the stress at the beam arch joint will gradually become stable. When the load reaches a certain value, the beam arch joint will enter the ultimate stress bearing stage, as can be seen from Figure 5 (b). The edge stress of the main beam reaches a maximum of 249.5MPa at the extension and junction of the arch rib. Figure 5 (c) shows that the stress at the root of the arch rib is distributed in a divergent manner from the middle to the periphery. At this stage, the beam arch joints may appear plastic hinge, resulting in large permanent deformation or even damage to the beam arch joints. After the load is removed, the deformation at the joint of the beam arch will gradually return to the original state. The deformation of the arch consolidated joint is the whole deformation under complex stress conditions, and the local deformation is not too large.

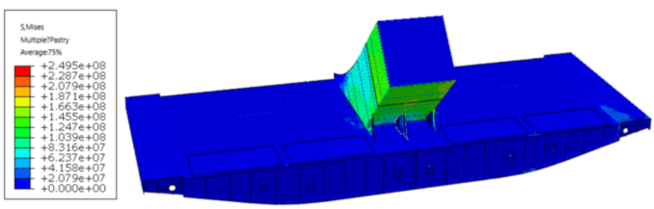

(a) Global stress variation cloud map

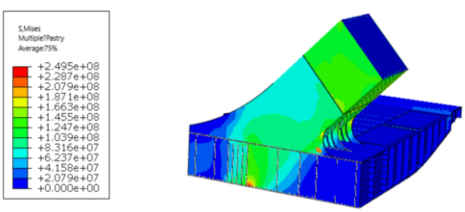

(b) Stress state of side web of main beam

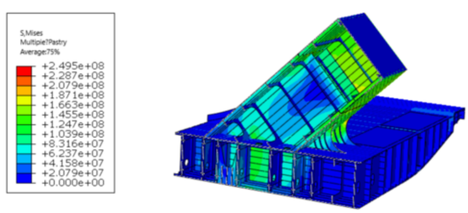

(c) Stress state of transverse diaphragm of main beam

Figure 5. Beam arch joint structure stress

4.2. Joint Deformation Analysis

The maximum displacement and stress nephogram were analyzed by intercepting the displacement and stress results in the model. The overall structural deformation of beam arch joints is shown in Figure 6. The deformation is exaggerated by 20 times, and the maximum deformation of the overall structure of the node is about 3.6cm. In Figure 6. The maximum deformation of the beam arch joint is large under this working condition, but there is no local deformation and no buckling phenomenon of the structure. Since the external force is directly input from the boundary section, the maximum deformation of the joint occurs at the boundary section. The joint deformation is the whole deformation, and there is no local buckling deformation.

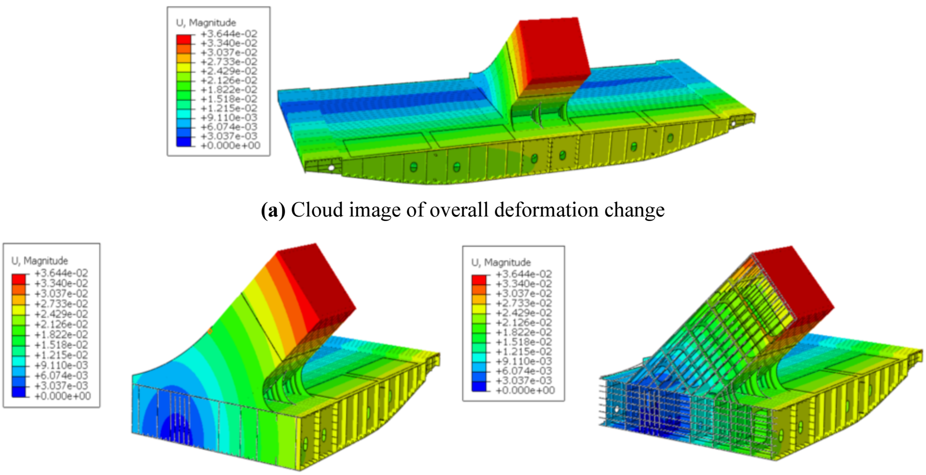

(a) Cloud image of overall deformation change

(b) Profile smooth cloud image

(c) Section plane physical cloud image

Figure 6. Structural deformation of beam arch joint

According to the finite element analysis results, in Figure 6. The beam arch joint will have a certain deflection deformation under the action of load. At this time, the shape of the flexural line of the beam arch joint is mainly determined by the magnitude and direction of the load. With the increase of load, the flexural deformation at the joint of beam arch tends to be stable gradually. At this stage, the shape of the flexure line of the beam arch joint is basically unchanged, but the amount of flexure will gradually increase. When the load reaches a certain value, the beam arch joint enters the stage of ultimate bearing capacity. This is shown in Figure 6. From the section diagram that the maximum deformation position is 3.6cm at the root of the arch rib, and the minimum deformation position is at the junction of the main beam and arch rib, and the overall trend is gradually increasing from the junction of the main beam and arch rib to the root of the arch rib.

4.3. Reliability Verification of Solid Finite Element Model

4.3.1 Experimental design

In order to ensure the safety of the main beam in the construction stage and the stress distribution of the main beam after the construction is in line with the design requirements, the local model experiment is carried out on the arch joint of the beam. The local model test is mainly to investigate the stress state of the arch foot under the most unfavorable working conditions. According to Saint-Venant's principle, if the surface force on the boundary of the small part of the body is transformed into a surface force with different distribution but equivalent experience (the principal vector is the same, and the principal moment is the same for the same point), then the stress distribution near will be significantly changed, but the effect far away is negligible. Therefore, the appropriate extension of the length of the bar can simulate the actual situation more accurately. The preliminary finite element analysis of the consolidated joint of the beam arch shows that the main possible overlimit location is above the support, so it is necessary to intercept the beam arch joint model of the local GJa section for test analysis. The experimental device design is shown in Figure 7.

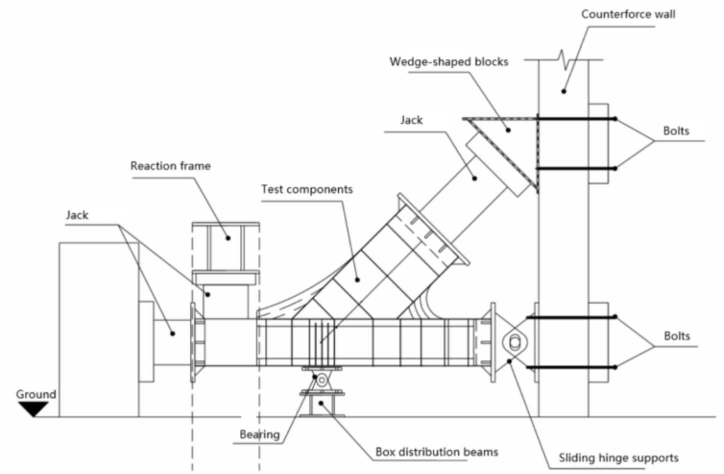

Figure 7. Design drawing of the design test device

The key of arch foot test model is to design a reaction system of arch foot model that can simulate the stress characteristics of arch foot in real bridge. In order to restore the actual situation of force transfer from arch rib to double box, the GJa segment model of single and double box member is extended. The arch rib extends from 4800mm to GL1 segment in original size, which is reflected in the extension of 960mm in single and double box member. The test model mainly adopts jack loading and matching counterweight blocks, etc. The specific loading device of the cast-in-place bridge panel is shown in Figure 8.

(a) Overall drawing of the loading device **(b)** Loading device local diagram

Figure 8. Loading device of cast-in-place bridge panel

4.3.2 Experimental process

In order to facilitate the analysis of stress distribution, the location of arch rib measurement points is determined as shown in Figure 9, which is divided into three measuring point sections along the arch rib axis. Due to the space limit of measuring point III section, no measuring points are arranged on GL-4 section.

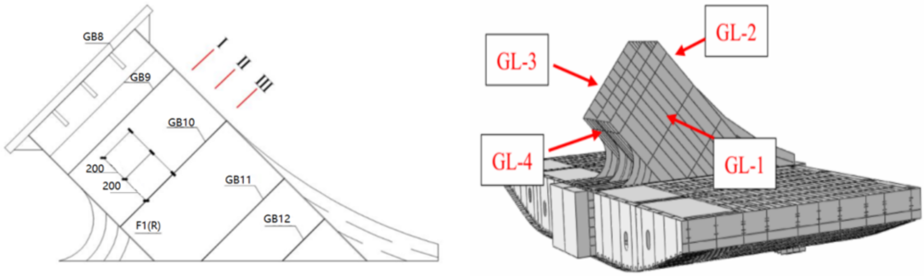

(a) Cross-sectional view of arch rib measurement point **(b)** Arch rib measuring point model

Figure 9. Location of arch rib measurement point

4.3.3. Analysis of experimental results

Based on the test results, the axial stress distribution law of the arch rib was analyzed, and the specific distribution law was shown in Figure 10. The stress distribution along the axial axis of the arch rib from the loading end presents a decreasing law, which conforms to the principle of Saint-Venant, and the maximum axial compressive stress is 194MPa, which is less than the design strength value of Q345 steel steel 305MPa, which meets the requirements of the code. At the same time, the stress of GL2 surface is greater than that of GL4 surface and GL1 surface is greater than that of GL3 surface because the arch rib jacks exert bending moment through eccentricity. To sum up, in the loading stage before the concrete pouring of the bridge panel, the arch rib under the ultimate load state of 1.2 times the bearing capacity is less than the strength design value of Q345 steel, and the structural force is reasonable and can meet the requirements of the code. The curve of force-strain relationship between the scaled test and the finite element is similar, and the difference is only 100με at most. The scaled test structure reflects that the general stress law of the structure is consistent with that of the finite element, which verifies the correctness of the scaled test and the finite element calculation.

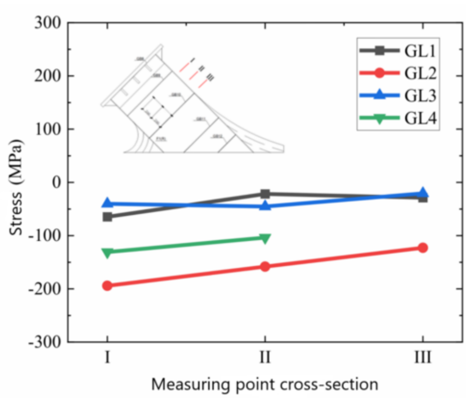

Figure 10. Stress distribution law of arch rib of 1:8 members before pouring concrete of bridge panel

5. Conclusion

It takes the large-span lower-carrying beam-arch composite Yuehu Special Bridge as the research object in the paper. Through the establishment of a three-dimensional finite element model and a scaled physical model, the stress state of the complex node part where the beam and arch are solidly connected is deeply analyzed. The reliability of the physical finite element model is verified by local model experiments, and the experimental results are consistent with the finite element analysis results, further proving the accuracy of the research method. The conclusion of this paper is as follows:

(1) the edge stress of the main beam reaches a maximum of 249.5Mpa at the point of extension and junction with the arch rib, and the stress at the root of the arch rib is distributed from the middle to the periphery; The maximum deformation position was 3.6cm at the root of the arch rib, and the minimum deformation position was at the junction of the main beam and the arch rib. The overall deformation showed a trend of increasing gradually from the junction of the main beam and the arch rib to the root of the arch rib.

(2) The force-strain curves of the scaled test and the finite element are similar, with a maximum difference of only 100με. The scaled test structure reflects that the overall stress law of the structure is consistent with that of the finite element, thus mutually verifying the correctness of the scaled test and the finite element calculation structure.

(3) In the case of applying 1.2 times the ultimate state load of bearing capacity, the test data are in good agreement with the finite element analysis results. There is no obvious buckling of the panel members of the cast-in-place bridge during the test, and no cracks appear on the concrete bridge panel. The arch rib yield failure test was completed when the load was loaded to the limit state of 1.8 bearing capacity. The axial stress at the arch rib failure exceeded the yield strength, and the rest were less than 345MPa. The results showed that the stress at the consolidated joints of the beam arch met the requirements.

The deficiency of this study is that stress concentration exists at the arch foot joints, especially at the joints between the tie beam and the beam and the arch rib and the tie beam, and the maximum stress value is close to the yield strength of the material, indicating that the safety reserve is low. These key areas require special attention and optimization in the design. New materials and innovative structural design, such as high-performance concrete and smart materials, should be explored to improve the bearing capacity and durability of Bridges, and smart sensor technology and Internet of Things technology should be combined to achieve real-time monitoring of key nodes of Bridges, timely warning and maintenance, and improve the safety and service life of Bridges.

References

[1] Xiong J Y, Shen Z Y. The rise of China's high-speed railway and the future development. Journal of transportation engineering, 2021, 21(5): 6-29.

[2] Kang Y J, Scordelis A C, Nonlinear analysis of prestressed concrete frames. Journal of the structural division, 1980, 106(2): 445-462.

[3] Sardone L, Sotiropoulos S. Computational design methods comparison for the optimization of variable section continuous beams//2024 IEEE International Workshop on Metrology for Living Environment (MetroLivEnv). IEEE, 2024: 373-378.
[4] Scattarreggia N, Salomone R, Moratti M, et al. Collapse analysis of the multi-span reinforced concrete arch bridge of Caprigliola, Italy. Engineering Structures, 2022, 251: 113375.
[5] Yuan H Q, Fan X C, Fan J F, et al. Iterative Advance Algorithm for arch rib lifting prediction of long-span concrete-filled steel tube arch Bridge. China Journal of Highway and Transportation, 2003, 16(3): 5.
[6] Zhang Z C. Research on Construction Control of long-span concreted-filled steel tube arch Bridge. Zhejiang University, 2004.
[7] Zhang Y Z. Research on Key Technologies of 128m Nelson System Simple Supported arch Bridge construction. Shijiazhuang Railway University, 2020.
[8] Long G, Zhu W, Liu Y, et al. Design and Analysis of Concrete-Filled Rectangular Steel Tubular Truss-Arch Composite Bridge Stiffened with PBL. Journal of Highway and Transportation Research and Development, 2020, 14(2): 57-66.
[9] Sun Q S, Miao J W. Research on Mechanical Performance of beam-arch Composite Bridge. China and Foreign Highway, 2016, 36(2):147-151.
[10] Zheng K H. Integral Analysis and arch foot Stress Study of long-span railway continuous beam-arch Composite Bridge. Southwest Jiaotong University, 2018.
[11] Dai G L, Wang Y. Seismic response characteristics of long-span railway continuous beam arch composite bridge. Journal of Railway Science and Engineering, 2015, 12(3): 557-563.
[12] Molner L, Tibaldo G. Comparative study of geometrical properties and preliminary design proposal for concrete arch bridges. Politecnico di Torino, 2021.
[13] Zhang Y. Design of large-span beam arch composite bridge for high-speed railway in High Intensity area. Railway Survey, 2020, 46(5): 129-133.
[14] Zhang Y, Zhu Y A, Su G M. Analysis of seismic Performance of m continuous beam-arch Bridge for high-speed railway (100+200+100). Railway Construction Technology, 2020, (5): 60-65.
[15] Gong G, Yu M. Spatial Stress Analysis of Block 0 of Continuous rigid frame Bridge. Highway Transportation Science and Technology, 2016, 33(6): 83-87, 94.
[16] Zhang F, Huang F Y, WANG Yan. Spatial Stress Analysis and Optimal Design of V-shaped Continuous rigid frame Bridge Block 0. Highway Transportation Science and Technology, 2019, 36(11): 59-67.
[17] Yu L S, Zhu D S. Analysis of local stress at consolidation point of tower girder pier of some Cable-stayed Bridges. Bridge Construction, 2008(1): 54-57.
[18] Petrosian L G. Vibrations of Combined Arch Systems: Rigid Beam-Flexible Arch//Dynamics of Structures: Oscillations/Vibrations. Cham: Springer Nature Switzerland, 2024: 391-424.
[19] Siwowski T, Zobel H, Al-Khafaji T, et al. The recently built polish large arch bridges–A review of construction technology. Archives of civil engineering, 2020, 66(4).
[20] Sun Z H, Teng L, Qin J Q. Force Analysis and Optimal Design of arch foot subdivision of Long-span concrete-filled steel tube trussed arch Bridge. China and Foreign Highway, 2020, 40(04): 141-146.